An Applet To Estimate The IOP-induced Stress and Strain Within the Optic Nerve Head.

Ian A. Sigal [A,*]

[A] Ocular Biomechanics Laboratory,
UPMC Eye Center, Eye and Ear Institute, Ophthalmology and Visual Science Research Center,
Department of Ophthalmology, University of Pittsburgh School of Medicine, Pittsburgh, PA

Short Title: Applet to estimate ONH biomechanics.

* **Correspondence**:
Ian A. Sigal, Ph.D.
Ocular Biomechanics Laboratory,
UPMC Eye Center, Eye and Ear Institute, Ophthalmology and Visual Science Research Center, Department of Ophthalmology, University of Pittsburgh School of Medicine, Pittsburgh, PA.
203 Lothrop Street, Rm 930, Pittsburgh PA, 15213.
email: sigalia@upmc.edu   phone: (412) 864-2220

For submission to IOVS

16 May, 2011

Abstract

Purpose: The ability to predict the biomechanical response of the optic nerve head (ONH) to IOP elevation holds great promise, yet remains elusive. The objective of this work was to introduce an approach to model ONH biomechanics which combines the ease of use and speed of analytical models with the flexibility and power of numerical models.

Methods: Models representing a variety of ONHs were produced, and finite element (FE) techniques used to predict the stresses (forces) and strains (relative deformations) induced on each of the models by IOP elevations (up to 10 mmHg). Multivariate regression was used to parameterize each biomechanical response as an analytical function. These functions were encoded into a flash-based applet. Applet utility was explored by investigating hypotheses concerning ONH biomechanics posited in the literature.

Results: All responses were parameterized well by polynomials (R^2 values between 0.985 and 0.999), demonstrating the effectiveness of our fitting approach. Previously published univariate results were reproduced with the applet in seconds. A few minutes allowed for multivariate analysis, with which it was predicted that often, but not always, larger eyes experience higher levels of stress and strain than smaller ones, even at the same IOP.

Conclusions: We have introduced an applet with which it is simple to make rapid estimates of IOP-related ONH biomechanics. The applet represents a step towards bringing the power of FE modeling beyond the specialized laboratory, and can thus help develop more refined biomechanics-based hypotheses. The applet is available for use at www.ocularbiomechanics.org.

Short description:

We introduce an applet with which it is fast and simple to estimate the biomechanical effects of intraocular pressure on the optic nerve head. We demonstrate the applet by using it to investigate hypotheses concerning optic nerve head biomechanics posited in the literature.

Introduction

Elevated intraocular pressure (IOP) is the primary risk factor for the development of glaucoma. There is, however, a wide range of sensitivities to IOP, wherein a substantial number of individuals with normal IOP develop the disease (normotensive glaucoma), whereas other individuals with elevated IOP show no signs of the neuropathy (ocular hypertension) [1,2]. Thus, it is important to understand the effects of IOP on the optic nerve head (ONH) and how this varies between individuals. Of particular interest are the effects on the lamina cribrosa (LC), a region within the ONH where insult to the retinal ganglion cell axons occurs early in the disease. Despite recent advances in ocular imaging, such as second harmonic imaging [3] and deep scanning OCT [4-6], direct measurement of the effects of IOP on the ONH remains a challenge. As a result, modeling has become a leading approach for studying ocular biomechanics.

Traditionally there have been two approaches to model the effects of IOP on the eye: analytical and numerical. Analytical models may be written as a mathematical expression. For example, Laplace's law (S= PR/2) relates the tension (S) on the wall of a spherical vessel to the magnitude of the pressure (P), the radius (R) and the thickness of the wall (t). Analytical models are attractive for their elegance and simplicity, since it is simple to enter values and compute predictions. The complexity in deriving closed form mathematical relationships, however, has meant that analytical models are limited to highly simplified geometries, material properties and loading conditions. Laplace's Law, for example, assumes a thin-walled sphere composed of a single material. These assumptions, while valid in some circumstances, are violated when there is an opening in the shell, such as the ONH. Hence Laplace's Law cannot be trusted to make valid predictions involving the ONH and peripapillary sclera. In contrast, numerical models such as those analyzed using the finite element (FE) method can incorporate more realistic geometries, materials and loadings than analytical models can and are generally easier to adapt to new conditions. Nonetheless, even relatively simple FE models can be difficult to produce and analyze, requiring particular expertise and specialized software. Consequently, the ability to predict and evaluate hypotheses of how an increase in IOP affects the biomechanics of the ONH in a simple manner that considers the complexity of the tissues continues to elude researchers.

The objective of this work was to introduce an approach to estimate the effects of IOP on the ONH which combines the ease of use and speed of analytical models with the flexibility and power of FE models. This approach uses surrogate models encoded in an applet. In the first part of

this manuscript we describe in detail what we mean by surrogate models, demonstrate how these can be developed for the ONH, and show how encoding these surrogate models into an applet produces a tool for estimating IOP-related ONH biomechanics. We show that predictions made with the applet are virtually identical to those previously obtained with standard FE modeling. In the second part of the manuscript we demonstrate the applet's usefulness by showing how it can be used to explore some questions on ONH biomechanics posed in the literature.

Methods

General strategy

The general strategy for producing the applet consisted of three steps: modeling, metamodeling and applet coding (Figure 1). In the modeling stage a parameterized FE model of the ONH was developed whereby model characteristics, such as the size of the eye, or the stiffness of the LC, could be varied by specifying a few parameters. 2094 variations of the model were made, representing a wide variety of ONHs. Each of these models was solved, that is, the mechanical effects of IOP on the particular ONH were predicted using the FE method. These effects were quantified as a set of outcome measures or responses, e.g. the maximum IOP-induced stretch within the LC. In the metamodeling step regression methods were used to fit a polynomial function to each of the responses as a function of the characteristics of the ONH (the parameters). A close fit indicated that the polynomial function effectively captured the relationship between the parameters and the response. The polynomial function is thus an analytical model of the population of FE models, a *metamodel*, and can be used as a surrogate in lieu of the actual FE models. Not surprisingly, obtaining a close fit required relatively long polynomial functions (more than 80 terms) which are inconvenient to use. Therefore in the third step, the polynomials were coded into an applet. The applet works as a black box, handling the calculations and shielding the user from the complexity of the polynomial functions. With the applet it is easy to enter a set of values for the parameters, thus defining an ONH, and almost instantly obtain predictions of the ONHs response to increases in IOP. The accuracy of the predictions made with the applet depends on the closeness of the fits, and the quality of the underlying FE models. For simplicity, the models and applet in this work are based on previously reported, and thoroughly discussed, simplified models [7-9]. Notwithstanding the simplifications, the applet is already more comprehensive than any analytical model of the ONH and much easier to use and orders of magnitude faster to compute than even the simplest FE models.

Modeling

The development, processing, simulation and analysis of the FE models are described elsewhere [7, 8]. For this study we selected 8 parameters (Table 1 and Figure 2), out of the 21 in the original models, based on a preliminary multivariate sensitivity analysis (results not shown). In the preliminary study it was found that the eight parameters, and their interactions, accounted for between 97.7 and 99.9% of the variance in the responses. For simplicity the applet presented in this manuscript are based on these eight parameters only, acknowledging that this implies an approximation of up to 2.3% in the variance relative to a model with 21 parameters. The 13 parameters not varied here were set at their baseline levels used in our previous work [7, 8]. All tissues were assumed linearly elastic, isotropic and homogeneous [7-10]. Tissue stiffnesses were defined by Young's moduli, and compressibilities by Poisson's ratios. All tissues, other than the pre-laminar neural tissue (PLNT), were assumed incompressible. In this work, stiff and compliant are used to describe high and low Young's moduli, respectively. Thus, stiffness is equivalent to the tissue's mechanical property and is independent of the geometry. The parameters and their ranges have been discussed in detail elsewhere [7-10]. The geometric parameters were defined as described elsewhere [7, 8].

The base model was defined to represent a low IOP (5 mmHg), and the IOP increases relatively small (up to 10 mmHg). The rationale for these choices and its consequences are addressed in the Discussion section. The apex of the anterior pole was constrained in all directions to prevent displacement or rotation. The effects of IOP were modeled as a distributed load acting on the surfaces exposed to the interior of the eye.

The response of each of the ONH models to increases in IOP was simulated using commercial FE software (Ansys 8, Ansys Inc, Canonsburg, PA). Twelve measures were used to characterize the response to IOP: As measures of deformation the maximum tensile and compressive strains, computed from the maximum and minimum principal strains respectively. As a measure of the forces borne by the tissue the equivalent Von Mises stress. For briefness, henceforth we refer to these as the tensile and compressive strains and stress. Each of these measures was computed within the LC and prelaminar tissue (within 7.5° of the axis of symmetry [7-9]), and characterized by the 50th and 95th percentiles, the median and peak [7-9]. To improve regression fits the responses were transformed, with the optimal transformation for each response determined using a Box-Cox analysis [11, 12]. For all responses it was found that the optimal transformation was a (natural) logarithm.

Metamodeling

Each combination of parameters defined a "configuration", or case. The combinations of parameters were chosen using a response surface methodology with 2094 combinations produced, simulated and analyzed (Figure 3). The configurations were pre-processed, simulated and analyzed automatically and in randomized order. Several cases were replicated to verify that there were no errors, such as drift, as it should be in deterministic analyses. The responses were then fit by polynomial functions f of the form:

$$\text{Response} = f(x_1, x_2, ..., x_n) = \beta_0 + \sum_{i=1}^{n} \beta_i x_i + \sum_{j=1}^{n} \sum_{i=1}^{j} \beta_{ij} x_i x_j + \sum_{k=1}^{n} \sum_{j=1}^{k} \sum_{i=1}^{j} \beta_{ijk} x_i x_j x_k + \varepsilon$$

where the x's are the factors, β's the regression coefficients to be estimated, and ε the residual. The coefficients represent the following: β_0 is the offset, β_i the linear factor effects, β_{ij} the two-factor interactions ($i \neq j$) or the quadratic factor effects ($i=j$), and β_{ijk} the higher-order interactions and the cubic factor effects (i=j=k). We evaluated whether it was necessary to use the full function, a third order polynomial, or if close fits could be obtained with reduced versions.

The number of ONHs analyzed was more than the minimum needed to fit the chosen polynomial, and in this sense the fit was overdefined. This was done so that after fitting, data were left to compute measures of quality of fit, i.e. how well the metamodel represented the responses as computed in the FE models. We computed the usual coefficient of determination (R^2), but this coefficient is susceptible to artifacts (e.g. its value increases with the number of data points or with the range of the data). Thus we also computed the adjusted and predited R^2, which are less sensitive to such artifacts [11, 13]. Additionally, the signal-to-noise ratio, as the ratio of the range of the predicted values to the average prediction error was calculated[11, 12]. Statistical design and analysis were carried out using specialized software (Design-Expert 7; Stat-Ease Inc, Minneapolis, MN).

Applet coding

The functional descriptions of the metamodels were integrated into a custom flash-based applet (Xcelsius 4.5, SAP, Germany).

Comparison with previous studies

The metamodels and applet developed in this work are more comprehensive than what we have reported [7-9], for example, capturing simultaneously factor interactions and cubic nonlinearities

in the responses. Nevertheless, the FE models used in this work were based on our previous models. Hence, it should be possible to reproduce with the applet the previous predictions in [8], albeit with the differences in IOP increase (up to 10 mmHg here and 25 mmHg previously). Thus, as a check on the applet we repeated one part of the sensitivity analysis in [8] and compared the results.

Demonstration cases

To demonstrate the usefulness of the applet introduced in this work we show how these applet can be used to explore the following questions about ONH biomechanics:

- **Eye size**. Do the ONHs of large eyes always experience higher stress and strain than the ONHs of small eyes, even when IOP is the same? This question has been raised several times, often in relation to the findings that myopia is a significant factor for the development of primary open-angle glaucoma, independent of IOP [14-18].

- **Uncertainty in LC mechanical properties**. Imaging and mechanical testing of ocular tissues continue to improve. Eventually it may be possible to determine in-vivo many of the characteristics of the ONH and sclera. Direct measurement of the mechanical properties of the LC, however, remains a challenge [19, 20]. Here we consider the following question: if all the characteristics of the ONH and sclera were known precisely, except for the mechanical properties of the LC, how much variability (uncertainty) would remain in the predicted IOP-induced stress/strain within the ONH?

Both issues can be explored with the applet using the same strategy: move the slider of the parameter of interest left/right (lowest/highest level) to "test" the effects on the predictions. Recall that the effects of the parameters are nonlinear and have interactions between them, i.e. that the effects of a parameter often depends on the other parameters [7, 20, 21]. Hence, the effects of one parameter need to be tested for many combinations of the other parameters. Our goal with this work was to demonstrate how the applet can be used to explore these questions, not to present a comprehensive analysis on the effects of either eye size or LC properties. Hence we varied the parameters in search of interactions using an arbitrary empirical search pattern guided by our experience.

Results

It was possible to fit all the responses closely using polynomial functions (Table 3 and Figure 4). The best fits were obtained with third order polynomials. The predicted R^2 values were between 0.985 and 0.999. Other measures of the quality of fit were also excellent, demonstrating that the fits capture the responses adequately and therefore that the polynomial functions can serve as surrogates for the FE models.

The polynomial functions were successfully implemented into an applet (Figure 5), for which response predictions were both rapid and easy to obtain.

Predictions made with the applet presented in this work were very close to those reported in the literature (Figure 6). This is further evidence that the analytical functions encoded in the applet are adequate surrogates for the FE models of [8], but that encoded as an applet are much simpler and faster to use. In [8] parameters effects were analyzed independently. The applet introduced here is much more flexible, making estimates for any combination of parameters within the ranges in Table 1.

Demonstration cases

Eye size: At the same IOP, higher tissue strains and stresses were predicted for larger eyes than for smaller eyes (Figure 7). This was the case for many, but not all, parameter combinations. Some parameter combinations were insensitive to the size of the eye, and a few others even resulted in lower peak strains and stress in larger eyes than smaller ones. However, for the vast majority of combinations, the strains and stresses within both the LC and prelaminar tissue responded in the same way to the variations in eye size, i.e. all increasing or all decreasing.

Uncertainty in LC mechanical properties: The predicted IOP-induced strains and stresses varied substantially depending on the properties of the LC (Table 3). Stiffer LCs always had lower strains and higher stress within the LC. The properties of the LC could have a substantial impact on the predicted strains and stress. For example, with every other parameter unchanged, the median Von mises stress could be six times larger (600% larger) in an eye with a stiff LC than in an eye with a compliant LC (27.6 mmHg vs. 4.6 mmHg). Similarly, the median tensile strain could increase more than fivefold (550% larger) in an eye with a soft LC compared with an eye with a stiff LC (strains of 0.94 % and 0.17%, respectively). When the LC modulus was more influential on stress it was less influential on strain, and vice versa.

Discussion

We have presented a methodology to produce an applet with which to estimate the biomechanical effects of elevation in IOP on the ONH. The applet, available for use at www.ocularbiomechanics.org, was based on producing surrogate models and integrating them into an applet. This applet combines the ease of use and speed of analytical models with the power and flexibility of FE models, and can be used to make predictions over a wide range of geometries and material properties. By considering these simultaneously, the resultant estimates incorporate parameter interactions and nonlinear effects, which can be substantial even in simplified models with linear materials. Predictions made with this applet corresponded well with the simpler versions in the literature. We also demonstrated how the applet can be used to explore questions about ONH biomechanics posed in the literature.

The originality of this work is twofold: to the best of our knowledge this is the first application of surrogate models in posterior pole biomechanics, and also the first implementation of FE-based surrogate biomechanical models into an applet. Surrogate models are convenient because they bypass the need to explicitly compute the source models (in this case FE models) while retaining the fundamentals of the response. When surrogate models are formulated in closed form, such as the polynomials used in this work, they also allow calculation of integrals and derivatives, which are useful to identify extreme or inflection points at relatively low computational cost [22, 23]. For these and other useful properties, surrogate models have seen application in several areas of engineering, where they are used in optimization [12, 23, 24].

The ability afforded by the applet to produce rapid estimates of the effects of IOP on the ONH is useful for evaluating hypotheses of sensitivity to IOP, as was demonstrated by the two examples provided. In the first example, we have shown that the models and applet predict that often, but not always, a small increase in IOP results in higher stresses and strains within the ONH in a larger eye than in a smaller one. Higher stresses and strains in larger eyes compared with smaller eyes have been hypothesized to be one of the reasons behind the increased risk for glaucoma associated with myopic eyes, independent of IOP [14-18]. Our results therefore support these hypotheses, but also predict a range of sensitivities due to other ocular characteristics. Specifically, it was predicted that IOP-induced stress and strain slightly decrease with increased eye size when the eyes have a thick and stiff sclera, a large canal size and soft neural and LC tissues. It is still unknown how often these characteristics occur simultaneously. Previous non-multivariate techniques for

computing the biomechanical effects of IOP on the ONH were incapable of making a prediction such as this. We point out that since the scleral shell was assumed spherical we varied eye diameter rather than axial length.

In the second example we have shown that uncertainty in LC mechanical properties translates into substantial uncertainty in the predictions of IOP-induced stress and strain within the LC, even if every other characteristic of the ONH and sclera considered by the model is known. This suggests that it is important to continue working towards characterizing LC properties, whether by measuring properties of the LC itself, or its covariations with other characteristics.

A further convenience for the applet users was the reduction in the number of parameters from 21 in the original models [7-9] to the 8 most influential ones. This was only discussed briefly here for simplicity, and because it was done using statistical techniques similar to those we have applied elsewhere [7, 21, 22]. Although we acknowledge that not accounting explicitly for 13 parameters implies an approximation of up to 2.3% in the variance, we believe that reducing the number of parameters by 61% was worthwhile, especially when considering that this reduces the number of two and three-factor interactions dramatically (by 98.78% and 99.99% respectively).

We recognize, however, a potential risk with the applet introduced here. Namely, that the ease of use may make it easy to dismiss the fundamental limitations of the underlying FE models, and their consequences. When interpreting predictions made with the applet it is critical to consider that the physiologic relevance and accuracy of the surrogate models and applet depend on the quality of the underlying FE models. There is no *a priori* reason to expect that a polynomial shall provide an adequate representation of the population of FE models. Here it was found that cubic polynomials allowed accurate representation of system behavior. The polynomials used as surrogate models should not be understood to be a mechanistic relationship, but rather an approximation of the responses dependence on the parameters within the ranges studied. George Box, the famous statistician, expressed this as [13]: "All models are wrong, but some are useful". Polynomials diverge and predictions outside the region of fit are unreliable.

For simplicity, the methodology and applet introduced and demonstrated in this work were based on simplified models of the ONH. We have discussed in depth the limitations and most salient consequences of the choices of model geometry and tissue mechanical properties [9, 25], of the parameters and their ranges [7, 8, 10], and of the responses analyzed [7, 8, 10, 26]. Hence, these will not be discussed at length again. Instead, we summarize earlier discussions, with a focus on the limitations and considerations most relevant to this work. The models represent only an acute deformation of

the tissues due to increases in IOP and do not account for the long-term remodeling processes that are known to take place as glaucoma develops [27-32]. The models do not account for LC microarchitecture, which may amplify the levels of strain [33], and do not consider the stresses at the baseline IOP. The models were based on a simplified axisymmetric geometry, and therefore do not completely reflect the complex architecture of the ONH region or the corneoscleral shell (which is not of constant thickness [34]). In addition, the ONH geometry differs between individuals in more complex ways that can be captured by the factors considered [35, 36].

The methodology can be extended to more complex FE models, although the number of models to prepare, run and analyze increases rapidly with the number of parameters in what is often referred to "the curse of dimensionality" [23]. In recent years there have been substantial advances in imaging and other experimental techniques, which have been applied to the posterior pole and ONH. [3, 6, 34, 37, 38] We are working to integrate these advances into improved FE models that incorporate more realistic anatomies (like the variations in scleral shell thickness [34, 39, 40]), material properties (anisotropic and nonlinear scleral properties [37, 41, 42], lamina cribrosa anisotropy and inhomogeneity [3, 19, 36]) and loading (larger IOP insult and cerebrospinal fluid pressure [43-47]). More complex models will require even more effort to produce and parameterize and have higher computational requirements. The time savings of surrogate models will be even greater in such models.

Despite the limitations the surrogate models and applet in this work are already more comprehensive than any analytical model of the ONH, and much easier and faster to use than even the simplest FE models. Also, the predictions are more directly applicable to the human ONH than Laplace's Law and Friedenwald's coefficient of rigidity [20].This study differs from most of the numerical studies of ONH biomechanics in that we analyzed relatively low levels of IOP (from 5 to 15 mmHg). We did this for several reasons: First, normal IOP is much more common than elevated IOP [1, 2], and therefore the analysis is relevant to a larger group. Second, there is better information on which to base the parameters and their ranges for normal eyes [9, 18, 31]. Third, small IOP elevations may be particularly informative in understanding the pathogenesis of low tension glaucoma. Further, as we have demonstrated before, ONH biomechanics are complex, even with simplified geometries and material properties [8, 9, 21, 26]. Simulating a relatively small IOP increase allowed us to use linear materials, whose stiffness can be specified by a single parameter for each tissue – the Young's modulus. Studies of ocular tissue properties have shown that while the assumption of linear scleral properties is reasonably adequate at low levels of IOP (under 10 mmHg), it becomes increasingly

problematic at elevated IOP (above 20 mmHg), because as the tissue stretches it stiffens [37, 41, 42, 48-51]. We believe that a solid understanding of ONH biomechanics at low pressures helps build up for understanding larger pressure increases.

We chose to analyze tensile and compressive strains and von Mises stress because studies in mechanobiology have suggested that these are potentially biologically relevant [52-57]. We have previously discussed the need to differentiate between tensile and compressive strains, as well as the value of computing peak and median levels of strain [26]. The LC is where insult to the retinal ganglion cell axons is believed to initiate in glaucoma [2, 58], whereas the PLNT is also of interest since it changes so dramatically during the development of glaucomatous neuropathy [35, 59, 60]. Work is underway on extending the responses analyzed to include other potentially biologically important measures of the effects of IOP (like the shearing strains [26, 61-63]), and those measurable in the experiment (such as LC displacement and canal expansion [6, 31, 35, 38, 64, 65]).

In summary, we have introduced an applet with which it is simple to make rapid estimates of IOP-related ONH biomechanics. We have demonstrated the use of the applet to explore questions posed in the literature. The applet represents a step towards bringing the power of FE modeling beyond the specialized laboratory, heightening appreciation of the factors influencing ONH biomechanics, and thus can help develop and refine biomechanics-based hypotheses.

Acknowledgements

Tables and Figures

Parameters and their ranges			
NAME	*UNITS*	*RANGE*	
		LOW	*HIGH*
Intraocular pressure increase [*]	mmHg	0	10
Internal radius of eye shell	mm	9.6	14.4
Scleral shell thickness	mm	0.64	0.96
LC anterior surface radius	mm	0.76	1.14
Poisson ratio of pre-laminar tissue	-	0.4	0.49
Lamina Cribrosa Young's Modulus	MPa	0.1	0.9
Sclera Young's Modulus	MPa	1	9
Neural tissue Young's Modulus	MPa	0.01	0.09

Table 1: Parameters and their ranges. See Figure 2 for factor definitions. * The responses were computed with respect to a baseline (reference) IOP of 5 mmHg.

Tissue	*LAMINA CRIBROSA*						*PRELAMINAR NEURAL TISSUE*					
Measure	*Strain*				*Stress*		*Strain*				*Stress*	
	Tensile		*Compressive*		*Von Mises*		*Tensile*		*Compressive*		*Von Mises*	
Percentile	*50th*	*95th*	*50th*	*95th*	*50th*	*95th*	*50th*	*95th*	*50th*	*95th*	*50th*	*95th*
R^2	0.998	0.988	0.999	0.994	0.999	0.996	0.996	0.987	0.999	0.995	0.998	0.994
Adjusted R^2	0.998	0.988	0.999	0.993	0.999	0.995	0.996	0.986	0.999	0.994	0.998	0.993
Predicted R^2	0.998	0.987	0.999	0.993	0.999	0.995	0.996	0.985	0.999	0.994	0.998	0.993
SSq Model	903.8	486.8	1074.6	751.2	1264.3	1493.2	667.8	401.2	578.7	493.6	1104.1	1094.2
SSq Residual	2.0	5.7	1.4	4.7	1.2	6.6	2.5	5.4	0.7	2.7	2.2	7.0
Residual %	0.2	1.2	0.1	0.6	0.1	0.4	0.4	1.3	0.1	0.6	0.2	0.6
SNR	435	189	598	257	706	333	281	179	582	273	522	295
PRESS	1.25	3.13	0.92	2.01	1.29	7.24	2.43	3.81	0.56	1.76	2.45	7.91
DOF Model	92	87	87	90	86	83	97	88	88	95	82	97
DOF Residual	1999	2004	2004	2001	2005	2008	1994	2003	2003	1996	2009	1994

Table 2: Measures of the quality of fit for the eight responses tracked. Multivariate regression methods were used to fit polynomial functions to the predicted response to increases in IOP in 2092 FE models. Excellent fits were obtained for all responses using cubic polynomials, as can be seen from the measures of in this table. See Figure 3 for more details of how other polynomial functions approximated a response. Of all the possible terms in the cubic polynomials only those terms that had a statistically significant ($p<0.0001$) contribution to the response were included in the regressions (DOF Model). The rest of the DOF were grouped as a measure of the residual (DOF Residual). DOF=Degrees of freedom, SSq = Sum of squares corrected by the mean, PRESS = Predicted residual sum of squares, SNR = Signal-to-noise ratio.

.

Example effects on the LC of uncertainty its own material properties					
Case with LC modulus influencing stress more than tensile strain					
Sclera modulus:	9 MPa	Neural tissue modulus:	0.09 Mpa	Sclera thickness:	0.8 mm
Eye radius:	14.4 mm	PLNT compressibility:	0.4	Canal size:	0.76 mm
		Median Von Mises stress		**Median Tensile strain**	
Soft LC (modulus 0.1 MPa)		4.6		0.33	
Stiff LC (modulus 0.9 MPa)		27.6		0.24	
Ratio of largest to smallest values		6		1.38	
Case with LC modulus influencing tensile strain more than stress					
Sclera modulus:	5 MPa	Neural tissue modulus:	0.01 Mpa	Sclera thickness:	0.96 mm
Eye radius:	9.6 mm	PLNT compressibility:	0.45	Canal size:	1.14 mm
		Median Von Mises stress		**Median Tensile strain**	
Soft LC (modulus 0.1 MPa)		9.5		0.94	
Stiff LC (modulus 0.9 MPa)		19.3		0.17	
Ratio of largest to smallest values		2		5.5	

Table 3. Using the applet to explore the effects of uncertainty in LC material properties on the stress and strain. If all the parameters were known precisely, except for the LC modulus, there would still be considerable variability in the IOP-induced stress and strain within the LC. This variability, however, depended on the case considered. Two cases are shown here, one where there was large variability in the stress and small variability in the strain, and another where it was the inverse. Not surprisingly softer LC's carry less load (lower stresses) and deform more (higher strains). All cases are shown at 10 mmHg, i.e. for an IOP increase of 5 mmHg over the baseline of 5 mmHg.
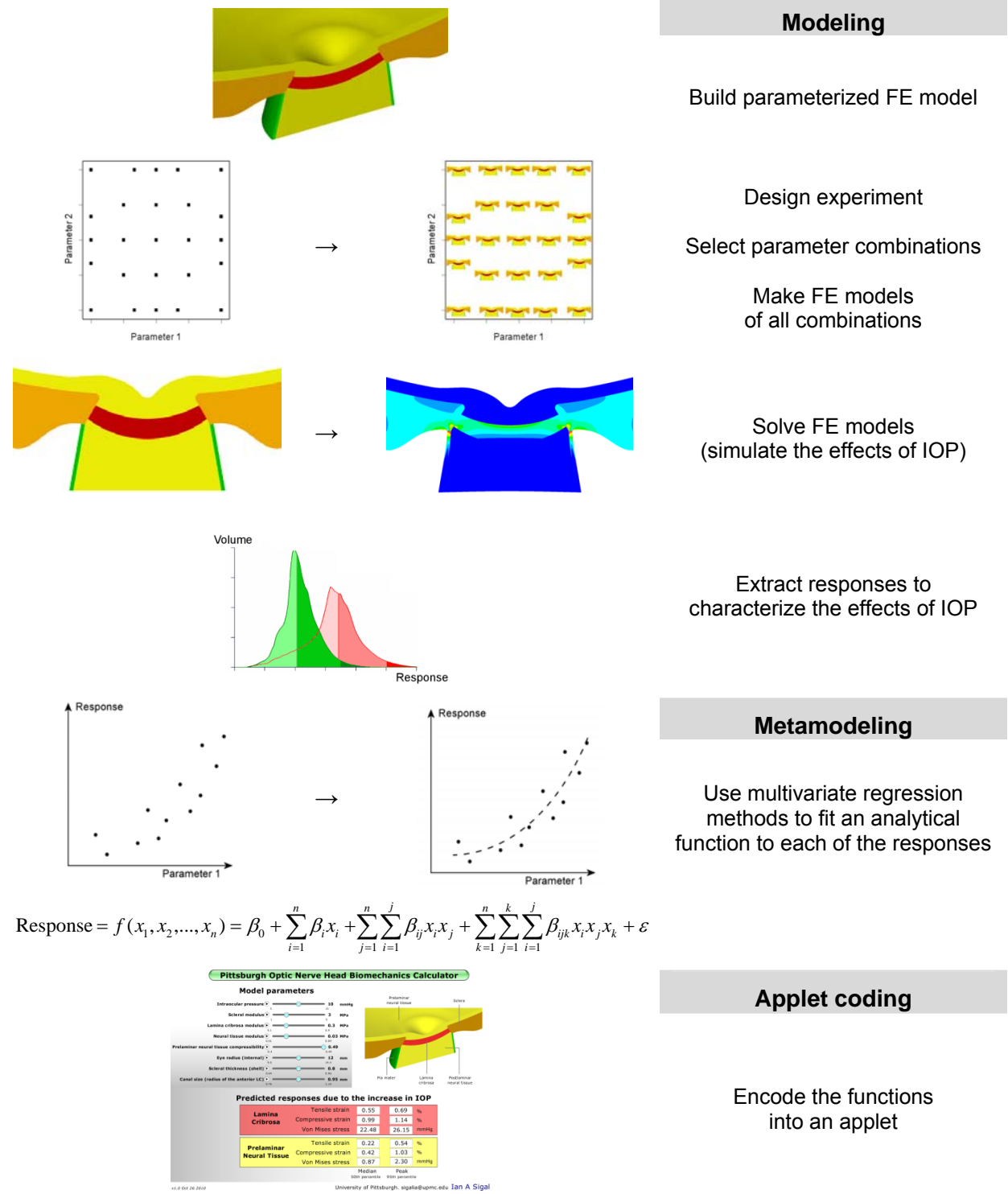
.

General strategy

Modeling

Build parameterized FE model

Design experiment

Select parameter combinations

Make FE models
of all combinations

Solve FE models
(simulate the effects of IOP)

Extract responses to
characterize the effects of IOP

Metamodeling

Use multivariate regression
methods to fit an analytical
function to each of the responses

$$\text{Response} = f(x_1, x_2, ..., x_n) = \beta_0 + \sum_{i=1}^{n} \beta_i x_i + \sum_{j=1}^{n}\sum_{i=1}^{j} \beta_{ij} x_i x_j + \sum_{k=1}^{n}\sum_{j=1}^{k}\sum_{i=1}^{j} \beta_{ijk} x_i x_j x_k + \varepsilon$$

Applet coding

Encode the functions
into an applet

Figure 1. General strategy. The study had three parts: modeling, metamodeling and applet coding.
Modeling: A parameterized FE model of the ONH was produced. An experimental design was
selected following a response surface method. The design prescribes the combinations of parameters

to be studied. An FE model was produced for each of the paramerter combinations, and the FE method used to predict the effects of an increase in IOP on the particular ONH model. These effects were characterized by a set of responses, or outcome measures. Metamodeling: Using multivariate linear regression an analytical function was fit to each of the responses as a function of the parameters. Cubic polynomials produced close fits, and can thus be used a surrogates, or *metamodels*, of the FE models. Applet coding: The polynomials had many terms and were cumbersome to use. To simplify their use these equations were encoded into a flash-based applet.
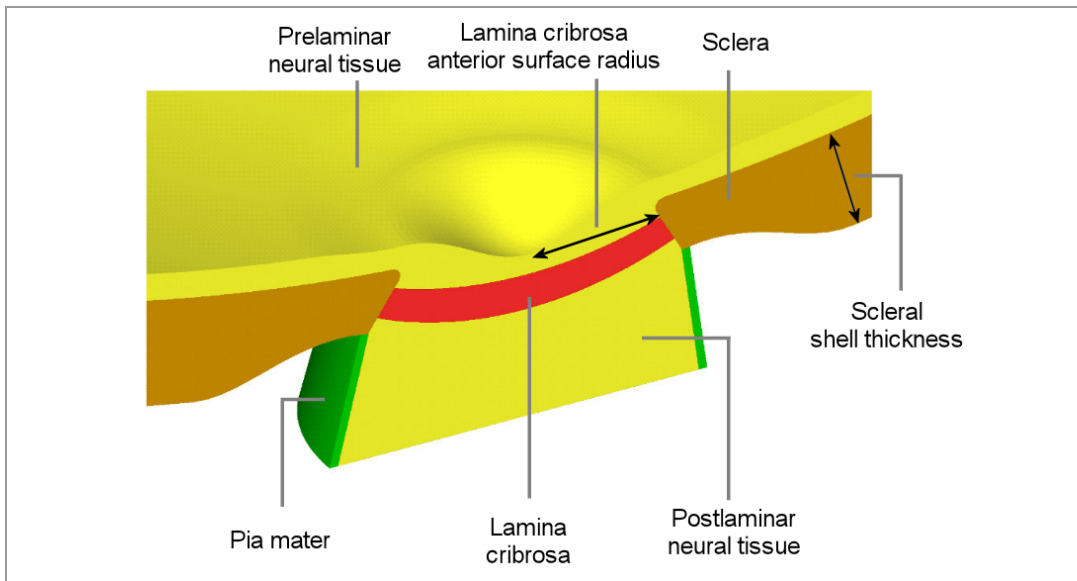
.

Figure 2. Model geometry. Five tissue regions were modeled: corneoscleral shell, lamina cribrosa (LC), prelaminar neural tissue (PLNT, including the retina and choroid), postlaminar neural tissue (ON, including the optic nerve), and pia mater. IOP was represented as a homogeneous force on the interior surfaces. The apex of the region representing the cornea was constrained in all directions to prevent displacement or rotation. See Table 1 for the factor ranges. Scleral thickness was parameterized over the shell, such that the scleral thickness at the canal wall remained unchanged. .
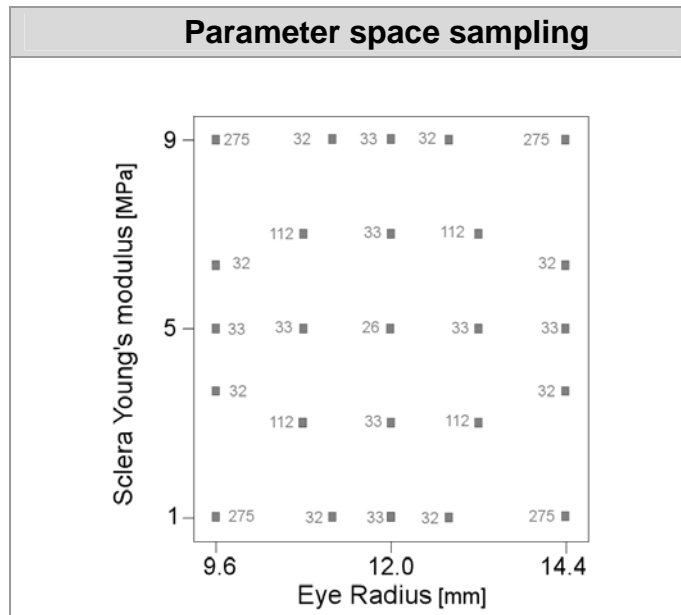
Figure 3. The combination of parameters used. Each small square represents a combination of parameters. Shown is a 2D projection onto the axes of Eye Radius and Sclera Young's moudlus. The number next to a square is the number of combinations that overlap in this projection. For example, 33 models were analyzed with an eye radius of 9.6 mm and sclera Young's modulus of 5 MPa. The 33 models varied in the other parameters. The sampling scheme was such that for any two parameters the 2D projection looks identical to the example shown here, for a total of 2094 models.
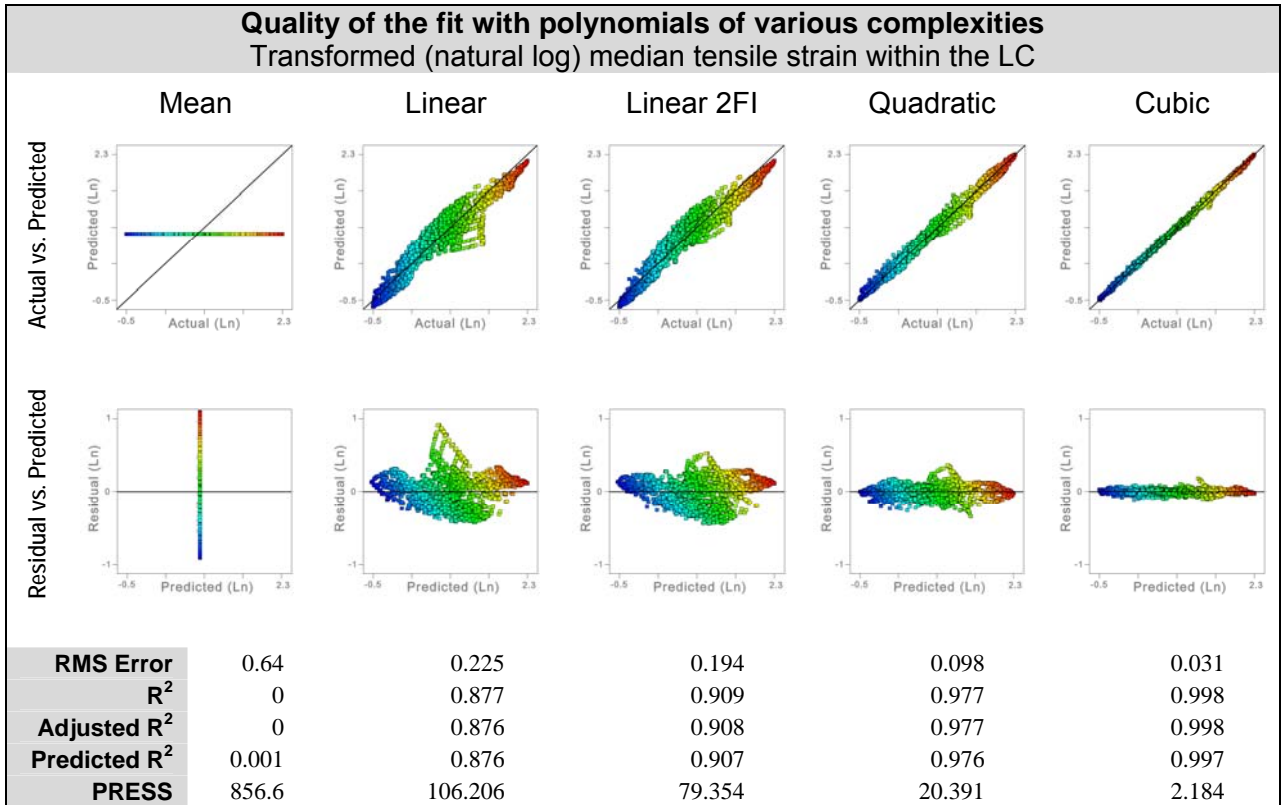
Quality of the fit with polynomials of various complexities
Transformed (natural log) median tensile strain within the LC

	Mean	Linear	Linear 2FI	Quadratic	Cubic
RMS Error	0.64	0.225	0.194	0.098	0.031
R^2	0	0.877	0.909	0.977	0.998
Adjusted R^2	0	0.876	0.908	0.977	0.998
Predicted R^2	0.001	0.876	0.907	0.976	0.997
PRESS	856.6	106.206	79.354	20.391	2.184

Figure 4. Multivariate regression was used to fit polynomials of various complexities to the predicted ONH response to increases in IOP in 2092 FE models. Obtaining a function suitable as a surrogate of the FE models required a close fit to the responses. The best fits were obtained with a cubic polynomial, followed by a quadratic polynomial, a linear polynomial with two-factor interactions (Linear 2FI), linear polynomial and finally by the mean (the simplest model possible). We show here the tensile strain within the LC as an example. All responses had a similar behavior. These results show that, at the points evaluated, cubic polynomials represent the FE models with less than 0.1% error. See Table 2 for measures of the quality of fit of cubic polynomials to all twelve responses analyzed. Shown are standard actual vs. predicted (top row) and residual vs. predicted (second row) plots. The fits were improved by first transforming the responses by a natural log. RMS = Root mean square, PRESS = Predicted residual sum of squares.
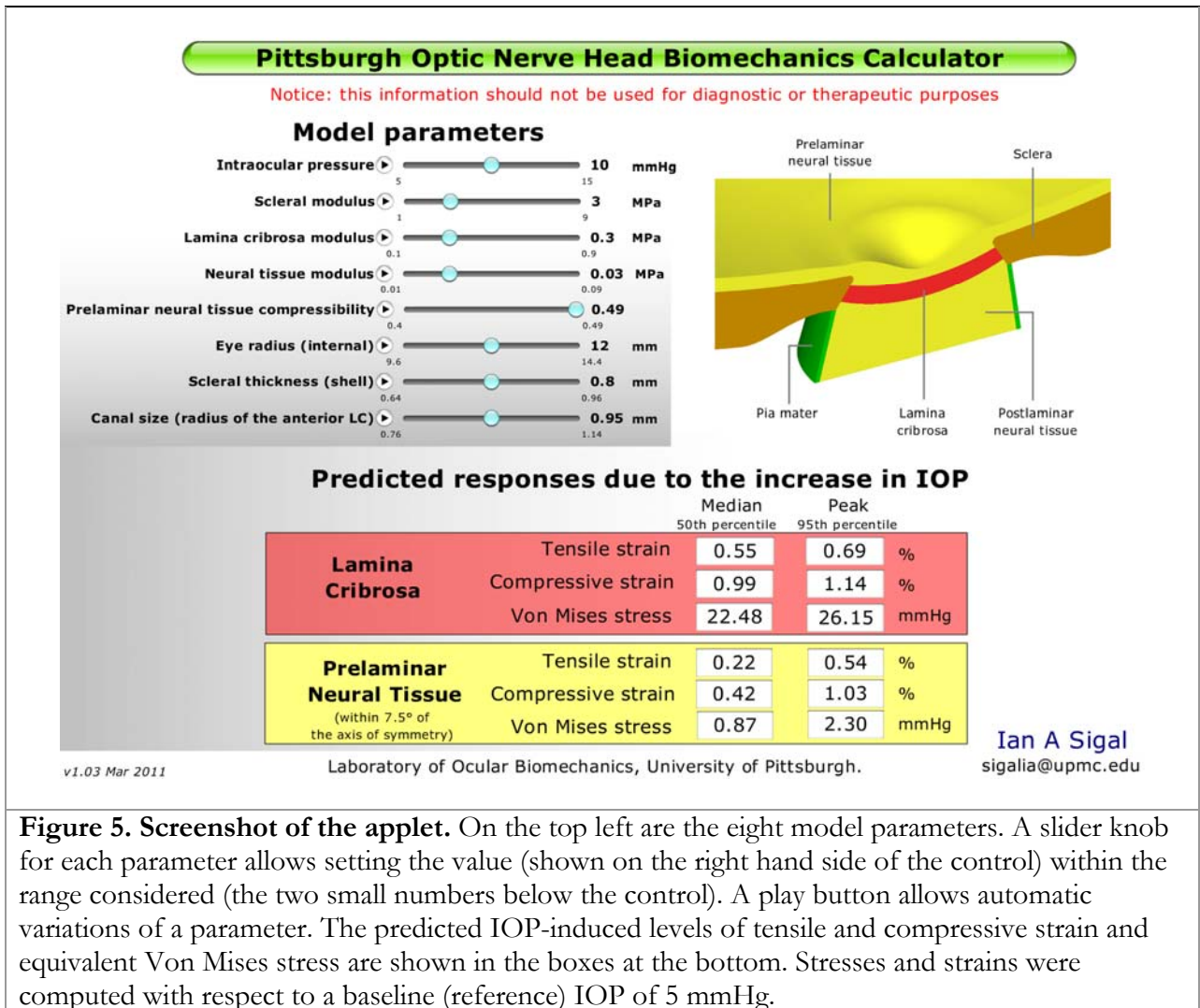
.

Figure 5. Screenshot of the applet. On the top left are the eight model parameters. A slider knob for each parameter allows setting the value (shown on the right hand side of the control) within the range considered (the two small numbers below the control). A play button allows automatic variations of a parameter. The predicted IOP-induced levels of tensile and compressive strain and equivalent Von Mises stress are shown in the boxes at the bottom. Stresses and strains were computed with respect to a baseline (reference) IOP of 5 mmHg.
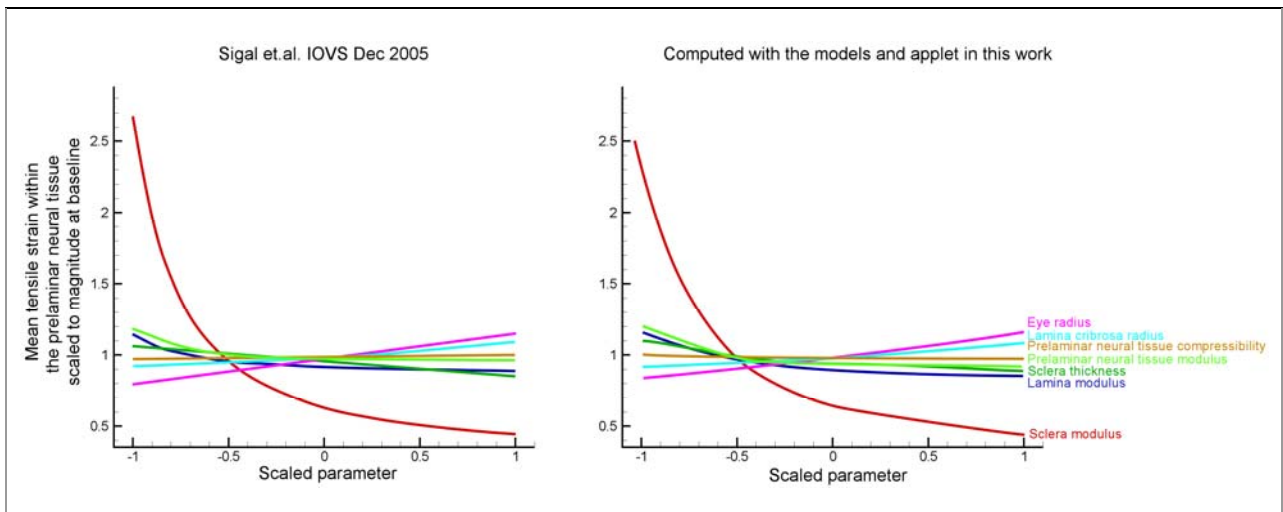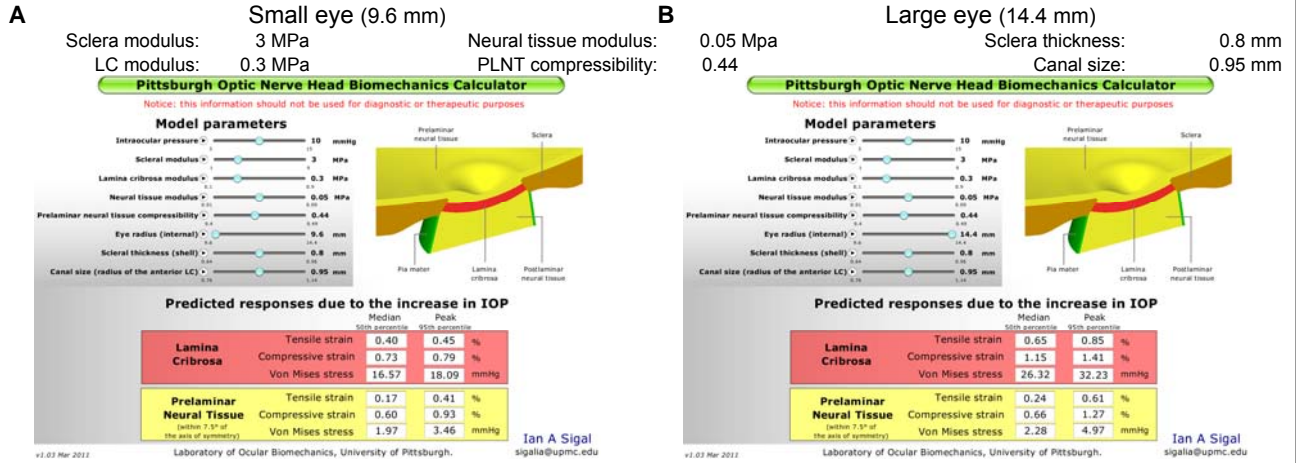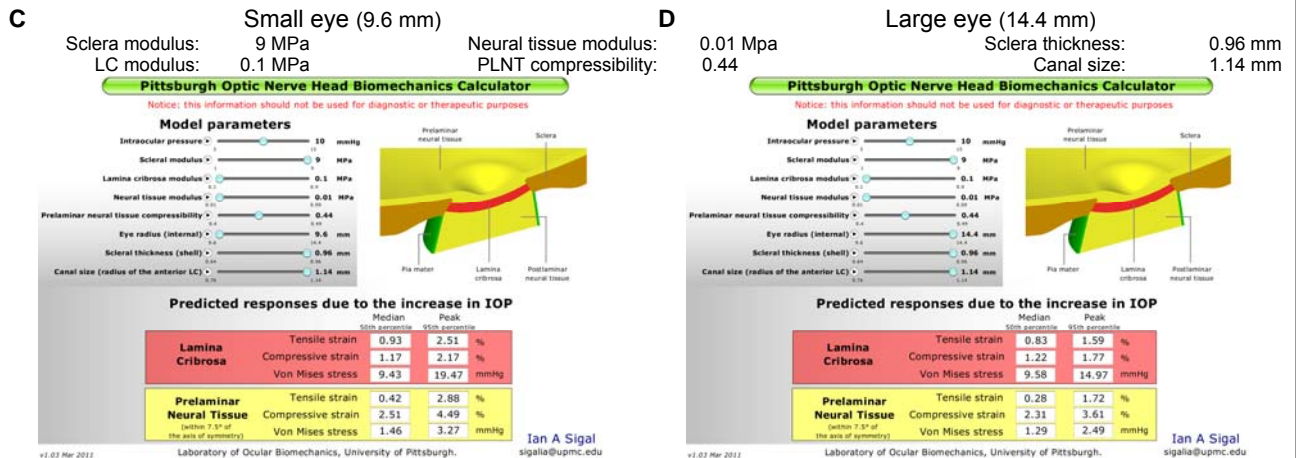
.

Figure 6. Comparison between the predictions obtained with the applet introduced in this work with those in the literature. There is excellent correspondence between the ONH response to IOP predicted using the models and applet in this work (right) with that in the literature (left) [8]. As before, to allow comparison of various factors on the same plot, the x-axes show each input factor value linearly scaled from its minimum value (-1) to its maximum value (1). Calculations with the applet were done for an IOP increase of 5 mmHg. The results from the literature have been adapted to include only the parameters varied in this work, and scaled in the y axis to compensate for the differences in IOP increases: 5 mmHg in this work versus 25 mmHg in the literature. Also note that previously the mechanical properties of the prelaminar and postlaminar neural tissue regions were varied independently, whereas in this work they were considered simultaneously as neural tissue. These results confirm that the applet introduced in this work reproduces previous work.

.

Example effects of eye size on ONH biomechanics

Common effect: larger eyes producing higher strains and stresses.

A — Small eye (9.6 mm)

| Sclera modulus: | 3 MPa | Neural tissue modulus: | 0.05 Mpa |
| LC modulus: | 0.3 MPa | PLNT compressibility: | 0.44 |

B — Large eye (14.4 mm)

| Sclera thickness: | 0.8 mm |
| Canal size: | 0.95 mm |

Uncommon effect: larger eyes producing slightly lower strains and stresses.

C — Small eye (9.6 mm)

| Sclera modulus: | 9 MPa | Neural tissue modulus: | 0.01 Mpa |
| LC modulus: | 0.1 MPa | PLNT compressibility: | 0.44 |

D — Large eye (14.4 mm)

| Sclera thickness: | 0.96 mm |
| Canal size: | 1.14 mm |

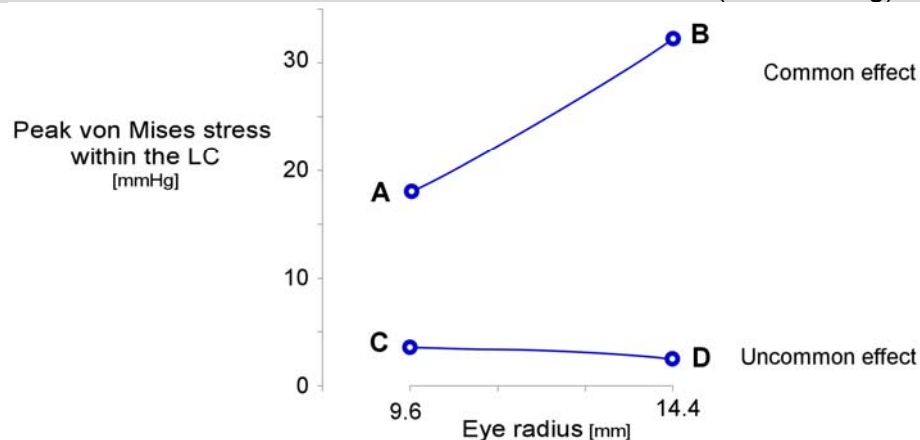## Peak von Mises stresses within the lamina cribrosa (at 10 mmHg)

.
Figure 7: Using the applet to explore the effects of eye size on stress and strain. With the applet it is simple and fast to explore the effects of eye size by moving the knob for the parameter "Eye radius" left/right (this is the sixth knob from the top). The effects of the parameters on ONH biomechanics are nonlinear and interact with each other. Hence the effect of the eye size varies depending on the other parameters. The common effect is that the LC and prelaminar neural tissue of a larger eye is subject to higher strains and stresses than those of a small eye (A and B). There are, however, cases where the same tissues are insensitive to eye size, and there may even be a small decrease in peak strain and stress with increasing eye size (C and D). The only difference between A and B, and between C and D is the eye radius. All cases are shown at 10 mmHg, i.e. for an IOP increase of 5 mmHg over the baseline of 5 mmHg.

References

1. Quigley HA. Number of people with glaucoma worldwide. Br J Ophthalmol 1996;80:389-393.
2. Quigley HA. Glaucoma: macrocosm to microcosm the Friedenwald lecture. Invest Ophthalmol Vis Sci 2005;46:2662-2670.
3. Brown DJ, Morishige N, Neekhra A, Minckler DS, Jester JV. Application of second harmonic imaging microscopy to assess structural changes in optic nerve head structure ex vivo. J Biomed Opt 2007;12:024029.
4. Drexler W, Morgner U, Ghanta RK, Kartner FX, Schuman JS, Fujimoto JG. Ultrahigh-resolution ophthalmic optical coherence tomography. Nat Med 2001;7:502-507.
5. Srinivasan VJ, Adler DC, Chen Y, et al. Ultrahigh-speed optical coherence tomography for three-dimensional and en face imaging of the retina and optic nerve head. Invest Ophthalmol Vis Sci 2008;49:5103-5110.
6. Strouthidis NG, Yang H, Fortune B, Downs JC, Burgoyne CF. Detection of optic nerve head neural canal opening within histomorphometric and spectral domain optical coherence tomography data sets. Invest Ophthalmol Vis Sci 2009;50:214-223.
7. Sigal IA. Interactions between geometry and mechanical properties on the optic nerve head. Invest Ophthalmol Vis Sci 2009;50:2785-2795.
8. Sigal IA, Flanagan JG, Ethier CR. Factors influencing optic nerve head biomechanics. Invest Ophthalmol Vis Sci 2005;46:4189-4199.
9. Sigal IA, Flanagan JG, Tertinegg I, Ethier CR. Finite element modeling of optic nerve head biomechanics. Invest Ophthalmol Vis Sci 2004;45:4378-4387.
10. Sigal IA, Flanagan JG, Tertinegg I, Ethier CR. Modeling individual-specific human optic nerve head biomechanics. Part II: influence of material properties. Biomech Model Mechanobiol 2009;8:99-109.
11. Montgomery DC. Design and Analysis of Experiments: Wiley; 2004:660.
12. Anderson MJ, Whitcomb PJ. RSM Simplified: Optimizing Processes Using Response Surface Methods for Design of Experiments: Productivity Press; 2005:292.
13. Box GEP, Hunter JS, Hunter WG. Statistics for experimenters: Design, Innovation, and Discovery. 2nd ed: Wiley-Interscience; 2005:664.
14. Fong DS, Epstein DL, Allingham RR. Glaucoma and myopia: are they related? Int Ophthalmol Clin 1990;30:215-218.
15. Mitchell P, Hourihan F, Sandbach J, Wang JJ. The relationship between glaucoma and myopia: the Blue Mountains Eye Study. Ophthalmology 1999;106:2010-2015.
16. Oku Y, Oku H, Park M, et al. Long axial length as risk factor for normal tension glaucoma. Graefes Arch Clin Exp Ophthalmol 2009;247:781-787.
17. Oliveira C, Harizman N, Girkin CA, et al. Axial length and optic disc size in normal eyes. Br J Ophthalmol 2007;91:37-39.
18. Jonas JB, Berenshtein E, Holbach L. Lamina cribrosa thickness and spatial relationships between intraocular space and cerebrospinal fluid space in highly myopic eyes. Invest Ophthalmol Vis Sci 2004;45:2660-2665.
19. Roberts MD, Liang Y, Sigal IA, et al. Correlation between local stress and strain and lamina cribrosa connective tissue volume fraction in normal monkey eyes. Invest Ophthalmol Vis Sci 2010;51:295-307.
20. Sigal IA, Ethier CR. Biomechanics of the optic nerve head. Exp Eye Res 2009;88:799-807.
21. Sigal IA, Yang H, Roberts MD, Burgoyne CF, Downs JC. IOP-induced lamina cribrosa displacement and scleral canal expansion: an analysis of factor interactions using parameterized eye-specific models. Invest Ophthalmol Vis Sci In Press.
22. Sigal IA, Whyne CM. Mesh morphing and response surface analysis: quantifying sensitivity of vertebral mechanical behavior. Ann Biomed Eng 2010;38:41-56.

23. Forrester AIJ, Keane AJ. Recent advances in surrogate-based optimization. Progress in Aerospace Sciences 2009;45:50-79.
24. Kleijnen JPC. Design and analysis of simulation experiments: Springer; 2007.
25. Sigal IA, Flanagan JG, Tertinegg I, Ethier CR. Modeling individual-specific human optic nerve head biomechanics. Part I: IOP-induced deformations and influence of geometry. Biomech Model Mechanobiol 2009;8:85-98.
26. Sigal IA, Flanagan JG, Tertinegg I, Ethier CR. Predicted extension, compression and shearing of optic nerve head tissues. Exp Eye Res 2007;85:312-322.
27. Morrison JC, Dorman-Pease ME, Dunkelberger GR, Quigley HA. Optic nerve head extracellular matrix in primary optic atrophy and experimental glaucoma. Arch Ophthalmol 1990;108:1020-1024.
28. Morrison JC, Johnson EC, Cepurna W, Jia L. Understanding mechanisms of pressure-induced optic nerve damage. Prog Retin Eye Res 2005;24:217-240.
29. Hernandez MR. The optic nerve head in glaucoma: role of astrocytes in tissue remodeling. Prog Retin Eye Res 2000;19:297-321.
30. Hernandez MR, Andrzejewska WM, Neufeld AH. Changes in the extracellular matrix of the human optic nerve head in primary open-angle glaucoma. Am J Ophthalmol 1990;109:180-188.
31. Sigal IA, Flanagan JG, Tertinegg I, Ethier CR. 3D morphometry of the human optic nerve head. Exp Eye Res 2010;90:70-80.
32. Crawford Downs J, Roberts MD, Sigal IA. Glaucomatous cupping of the lamina cribrosa: A review of the evidence for active progressive remodeling as a mechanism. Exp Eye Res In Press.
33. Kodiyalam S, Roberts MD, Sigal IA, Hart RT, Burgoyne CF, Downs JC. Relative Contributions of Direct IOP and Scleral Canal Expansion on the Biomechanics of the Lamina Cribrosa (LC) of a Normal Monkey Eye. Meeting of the Association for Research in Vision and Ophthalmology. Ft Lauderdale; 2009.
34. Norman RE, Flanagan JG, Rausch SM, et al. Dimensions of the human sclera: Thickness measurement and regional changes with axial length. Exp Eye Res 2010;90:277-284.
35. Yang H, Downs JC, Girkin C, et al. 3-D Histomorphometry of the Normal and Early Glaucomatous Monkey Optic Nerve Head: Lamina Cribrosa and Peripapillary Scleral Position and Thickness. Invest Ophthalmol Vis Sci 2007;48:4597-4607.
36. Roberts MD, Grau V, Grimm J, et al. Remodeling of the connective tissue microarchitecture of the lamina cribrosa in early experimental glaucoma. Invest Ophthalmol Vis Sci 2009;50:681-690.
37. Girard MJ, Suh JK, Bottlang M, Burgoyne CF, Downs JC. Scleral Biomechanics in the Aging Monkey Eye. Invest Ophthalmol Vis Sci 2009.
38. Agoumi Y, Artes PH, Nicolela MT, Chauhan BC. Spectral Domain Optical Coherence Tomography Measurements of Laminar and Prelaminar Tissue Movement After Intraocular Pressure Elevation. E-Abstract 4898-A295. In: Sci IOV (ed), ARVO. Ft. Lauderdale; 2009.
39. Downs JC, Blidner RA, Bellezza AJ, Thompson HW, Hart RT, Burgoyne CF. Peripapillary scleral thickness in perfusion-fixed normal monkey eyes. Invest Ophthalmol Vis Sci 2002;43:2229-2235.
40. Downs JC, Ensor ME, Bellezza AJ, Thompson HW, Hart RT, Burgoyne CF. Posterior scleral thickness in perfusion-fixed normal and early-glaucoma monkey eyes. Invest Ophthalmol Vis Sci 2001;42:3202-3208.
41. Grytz R, Meschke G, Jonas JB. The collagen fibril architecture in the lamina cribrosa and peripapillary sclera predicted by a computational remodeling approach. Biomech Model Mechanobiol In Press.
42. Grytz R, Meschke G. Constitutive modeling of crimped collagen fibrils in soft tissues. J Mech Behav Biomed Mater 2009;2:522-533.
43. Berdahl JP, Allingham RR, Johnson DH. Cerebrospinal fluid pressure is decreased in primary open-angle glaucoma. Ophthalmology 2008;115:763-768.
44. Balaratnasingam C, Morgan WH, Johnstone V, Pandav SS, Cringle SJ, Yu DY. Histomorphometric measurements in human and dog optic nerve and an estimation of optic nerve pressure gradients in human. Exp Eye Res 2009;89:618-628.

45. Morgan WH, Yu DY, Alder VA, et al. The correlation between cerebrospinal fluid pressure and retrolaminar tissue pressure. Invest Ophthalmol Vis Sci 1998;39:1419-1428.
46. Morgan WH, Yu DY, Cooper RL, Alder VA, Cringle SJ, Constable IJ. The influence of cerebrospinal fluid pressure on the lamina cribrosa tissue pressure gradient. Invest Ophthalmol Vis Sci 1995;36:1163-1172.
47. Ren R, Jonas JB, Tian G, et al. Cerebrospinal fluid pressure in glaucoma: a prospective study. Ophthalmology 2010;117:259-266.
48. Girard MJ, Downs JC, Bottlang M, Burgoyne CF, Suh JK. Peripapillary and posterior scleral mechanics--part II: experimental and inverse finite element characterization. J Biomech Eng 2009;131:051012.
49. Elsheikh A, Geraghty B, Alhasso D, Knappett J, Campanelli M, Rama P. Regional variation in the biomechanical properties of the human sclera. Exp Eye Res 90:624-633.
50. Spoerl E, Boehm AG, Pillunat LE. The influence of various substances on the biomechanical behavior of lamina cribrosa and peripapillary sclera. Invest Ophthalmol Vis Sci 2005;46:1286-1290.
51. Woo SL, Kobayashi AS, Schlegel WA, Lawrence C. Nonlinear material properties of intact cornea and sclera. Exp Eye Res 1972;14:29-39.
52. Edwards ME, Wang SS, Good TA. Role of viscoelastic properties of differentiated SH-SY5Y human neuroblastoma cells in cyclic shear stress injury. Biotechnol Prog 2001;17:760-767.
53. Tan JC, Kalapesi FB, Coroneo MT. Mechanosensitivity and the eye: cells coping with the pressure. Br J Ophthalmol 2006;90:383-388.
54. Wang JH, Thampatty BP. An introductory review of cell mechanobiology. Biomech Model Mechanobiol 2006;5:1-16.
55. Ellis EF, McKinney JS, Willoughby KA, Liang S, Povlishock JT. A new model for rapid stretch-induced injury of cells in culture: characterization of the model using astrocytes. J Neurotrauma 1995;12:325-339.
56. Hernandez MR, Luo XX, Igoe F, Neufeld AH. Extracellular matrix of the human lamina cribrosa. Am J Ophthalmol 1987;104:567-576.
57. Rogers R, Culp-Stewart S, Flanagan JG. The Mechanobiologic Response of Optic Nerve Head Cells to Mechanical Strain. Meeting of the Association for Research in Vision and Ophthalmology. Ft. Lauderdale Florida; 2009.
58. Quigley HA, Addicks EM, Green WR, Maumenee AE. Optic nerve damage in human glaucoma. II. The site of injury and susceptibility to damage. Arch Ophthalmol 1981;99:635-649.
59. Yang H, Downs JC, Bellezza A, Thompson H, Burgoyne CF. 3-D histomorphometry of the normal and early glaucomatous monkey optic nerve head: prelaminar neural tissues and cupping. Invest Ophthalmol Vis Sci 2007;48:5068-5084.
60. Burgoyne CF, Downs JC, Bellezza AJ, Suh JK, Hart RT. The optic nerve head as a biomechanical structure: a new paradigm for understanding the role of IOP-related stress and strain in the pathophysiology of glaucomatous optic nerve head damage. Prog Retin Eye Res 2005;24:39-73.
61. Kirwan RP, Fenerty CH, Crean JK, Wordinger RJ, Clark AF, O'Brien CJ. Influence of cyclical mechanical strain on extracellular matrix gene expression in human lamina cribrosa cells in vitro. Mol Vis 2005;11:798-810.
62. Neufeld AH, Sawada A, Becker B. Inhibition of nitric-oxide synthase 2 by aminoguanidine provides neuroprotection of retinal ganglion cells in a rat model of chronic glaucoma. Proc Natl Acad Sci U S A 1999;96:9944-9948.
63. Ostrow LW, Langan TJ, Sachs F. Stretch-induced endothelin-1 production by astrocytes. J Cardiovasc Pharmacol 2000;36:S274-277.
64. Fortune B, Yang H, Strouthidis NG, et al. The effect of acute intraocular pressure elevation on peripapillary retinal thickness, retinal nerve fiber layer thickness, and retardance. Invest Ophthalmol Vis Sci 2009;50:4719-4726.
65. Yang H, Downs JC, Burgoyne CF. Physiologic intereye differences in monkey optic nerve head architecture and their relation to changes in early experimental glaucoma. Invest Ophthalmol Vis Sci 2009;50:224-234.